

Correction for acoustic attenuation effects in optoacoustic tomographic reconstructions

X Luís Deán-Ben, Daniel Razansky and Vasilis Ntziachristos*

Institute for Biological and Medical Imaging, Technical University of Munich and Helmholtz Center Munich, Ingolstädter Landstraße 1, 85764 Neuherberg, Germany.

ABSTRACT

The feasibility of correcting for the effects of acoustic attenuation in optoacoustic tomographic reconstructions obtained with model-based inversion is shown in this work. Acoustic attenuation is a physical phenomenon that takes place inevitably in actual acoustic media and becomes significant at high ultrasonic frequencies. The frequency dependence of acoustic attenuation and the associated dispersion lead to reduction of amplitude and broadening of the optoacoustic signals, which in turn cause, respectively, quantification errors and loss of resolution in the reconstructed images. In this work we imaged an agar phantom with embedded microparticles in three different scenarios, namely with the signals acquired with no attenuation, with the signals collected by placing an attenuating sample in between the phantom and the ultrasonic transducer and with the signals corrected for the effects of acoustic attenuation. The results obtained show that the quantification inaccuracies and the loss of resolution of the images can be partially corrected at the expense of introducing noise at high spatial frequencies due to the amplification of the high frequency components of the noise in the signals.

Keywords: Optoacoustic tomography, model-based inversion, acoustic attenuation

1. INTRODUCTION

Optoacoustics is an emerging modality with demonstrated capability of quantitative anatomical, functional and molecular imaging within depths of several millimetres to centimetres of tissue.¹⁻³ The quantitative nature of the technique relates to the measurement of the absorption of light by tissue chromophores, which provide high contrast, and its resolution derives from the measured ultrasonic signals.⁴ In optoacoustics, the illumination of the sample is usually performed by a short-pulsed laser, in a way that thermal confinement conditions are verified and instantaneous expansion can be assumed. Then, the optoacoustic reconstruction consists of calculating the initial pressure, which is proportional to the optical absorbed energy, from the measured pressure at several positions outside the sample.

Several algorithms have been reported to perform the optoacoustic reconstruction, in which for simplicity an homogeneous, non-attenuating acoustic medium is commonly assumed.⁵⁻⁸ Thereby, the quality of the images can be significantly reduced when this hypothesis is not valid. For example, acoustic heterogeneities cause time-shifting of the optoacoustic signals and/or their distortion due to reflected or scattered waves depending on the degree of acoustic mismatch.^{9,10} Thus, several modifications of the reconstruction algorithms, which take into account the presence acoustic heterogeneities, have been reported to reduce the respective distortion effects in the images.⁹⁻¹³

A different phenomenon that becomes significant at high frequencies in actual media is the acoustic attenuation of the ultrasonic waves.¹⁴ Acoustic attenuation is frequency dependent, as a result, the optoacoustic signals not only are reduced in amplitude as the ultrasonic wave propagates, but they also change shape, so that the reconstructed images obtained with algorithms in which a non-attenuating medium is assumed may be distorted. The reduction of amplitude of the ultrasonic waves causes quantification errors in the measured distribution of the optical absorption coefficient and a limitation in the achievable depth. Usually, it is the optical attenuation, rather than the acoustical attenuation, which determines such depth limit. However, at high frequencies, the

*E-mail: vntziachristos@gmail.com

effect of acoustic attenuation can become dominant and must be considered. On the other hand, the frequency-dependent reduction of amplitude also leads to dispersion of the acoustic waves in order to guarantee causality.¹⁵ Thereby, the optoacoustic wave pulses broaden as they propagate,^{16,17} which in turn causes loss of resolution of the reconstructed images. The resolution of the images depends on the available frequency content of the ultrasonic signals used to make the reconstruction, which is also affected by other factors apart from the acoustic attenuation. For example, the frequency response of the transducer or the filtering of the measured signals also contribute to the broadening in practical situations and often their effects are higher than the effect of acoustic attenuation.¹⁸

In optoacoustics, the frequency bandwidth of the signals is very broad, typically ranging from 50 Hz to 50 MHz.¹⁹ Then, it is important to correct for the effects of acoustic attenuation in the measured time-domain signals, namely reduction of amplitude and increment of the width (broadening). The reduction of amplitude is due to the frequency dependence of the attenuation coefficient and the broadening of the signals is caused by both such frequency dependence and the dispersion of the ultrasonic waves. In Ref. 18, we show that for media with a linear dependence of the attenuation coefficient the dispersion of the waves can be neglected in the correction, as no significant improvement in terms of correction of amplitude and width is achieved.

In this work, we analyse the improvement in the tomographic reconstructions obtained with a quantitative model-based algorithm developed at our group when the signals are corrected for the effects of acoustic attenuation. Experimental results with an agar phantom with embedded microspheres allow visualizing the improvement of the reconstructed image in terms of quantification accuracy and resolution.

2. MODEL-BASED INVERSION

We explain in this section the principles of the model-based inversion algorithm used to obtain the tomographic reconstructions.

The duration of the pulse employed in short-pulsed laser illumination is significantly lower than the thermal confinement time. Under these conditions, the temporal dependence of the absorbed energy can be approximated by a Dirac delta $\delta(t)$ and the generated pressure field in a homogeneous acoustic medium verifies

$$\frac{\partial^2 p(\mathbf{r}, t)}{\partial t^2} - c^2 \nabla^2 p(\mathbf{r}, t) = \Gamma H(\mathbf{r}) \frac{\partial \delta(t)}{\partial t}, \quad (1)$$

where c is the speed of sound, $H(\mathbf{r})$ is the amount of energy absorbed in the tissue per unit volume and Γ is the dimensionless Grueneisen parameter. A solution of Eq. 1 is given by the Poisson-type integral as

$$p(\mathbf{r}, t) = \frac{\Gamma}{4\pi c} \frac{\partial}{\partial t} \int_{S'} \frac{H(\mathbf{r}')}{|\mathbf{r} - \mathbf{r}'|} dS', \quad (2)$$

where S' is the surface of a sphere centred at \mathbf{r} and with a radius equal to ct . In a two-dimensional geometry, for which all the sources lie in a plane, the integration in Eq. 2 is performed over a circumference L' . In such case, the pressure in arbitrary units is expressed as follows

$$p(\mathbf{r}, t) = \frac{\partial}{\partial t} \int_{L'} \frac{H(\mathbf{r}')}{|\mathbf{r} - \mathbf{r}'|} dL', \quad (3)$$

where all the constants are dropped for simplicity. The two-dimensional approximation is valid, for example, when the illumination on the surface of the object lies in a plane and the scattering of light in the object is not significant or when imaging within the depth of focus of cylindrically-focused ultrasonic transducers. In those cases, the acoustic sources are mainly located at points close to the imaging slice.

The model-based inversion is based on a convenient discretization of Eq. 3 by considering the optical absorbed energy at the positions of the pixels in the region of interest (ROI) where the reconstruction is made. In a first step, a numerical approximation for the time derivative is used, so that Eq. 3 is expressed as follows

$$p(\mathbf{r}, t) \approx \frac{I(t + \Delta t) - I(t - \Delta t)}{2\Delta t}, \quad (4)$$

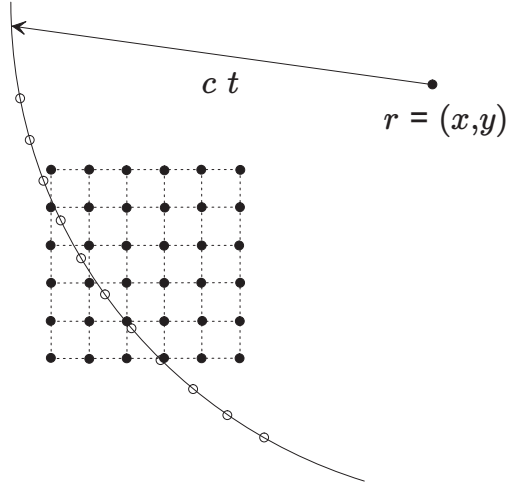


Figure 1. Principle of model-based inversion. The solid circles represent the grid of points corresponding to the position of the pixels of the ROI. The hollow circles represent a discretization of the curve along which the integral in Eq. 3 is performed.

being

$$I(t) = \int_{L'} \frac{H(\mathbf{r}')}{|\mathbf{r} - \mathbf{r}'|} dL'. \quad (5)$$

The discretization of Eq. 5 is performed by approximating a segment of the curve L' covering the whole ROI by a set of M equally-spaced points as shown in Fig. 1. The integral $I(t)$ is then calculated from the M points with positions \mathbf{r}'_l (hollow circles in Fig. 1) as

$$I(t) \approx \frac{d}{2} \sum_{l=1}^{M-1} \left[\frac{H(\mathbf{r}'_l)}{|\mathbf{r} - \mathbf{r}'_l|} + \frac{H(\mathbf{r}'_{l+1})}{|\mathbf{r} - \mathbf{r}'_{l+1}|} \right], \quad (6)$$

where d is the distance between two consecutive points. By combining Eqs. 4 and 6, Eq. 3 can be approximated as a linear combination of the optical absorbed energy at the points \mathbf{r}'_l . The value of $H(\mathbf{r}'_l)$ can be obtained by means of interpolation from the values of $H(\mathbf{r}'_k)$, being \mathbf{r}'_k the positions of the pixels of the ROI (solid circles in Fig. 1). In our case, we use bilinear interpolation considering the four neighbouring points (Fig. 2), so that

$$H(\mathbf{r}'_l) \approx (1 - \Delta x'_a)(1 - \Delta y'_a)H(\mathbf{r}'_a) + \Delta x'_b(1 - \Delta y'_b)H(\mathbf{r}'_b) + (1 - \Delta x'_c)\Delta y'_cH(\mathbf{r}'_c) + \Delta x'_d\Delta y'_dH(\mathbf{r}'_d), \quad (7)$$

being $\Delta x'_k = (x' - x'_k)/(x'_{k+1} - x'_k)$ and $\Delta y'_k = (y' - y'_k)/(y'_{k+1} - y'_k)$.

Then, the pressure $p(\mathbf{r}_i, t_j)$ measured at \mathbf{r}_i for instant t_j can be expressed as a linear combination of the absorbed energy per unit volume at the positions \mathbf{r}'_k of the pixels in the ROI, i.e.,

$$p(\mathbf{r}_i, t_j) \approx \sum_{k=1}^N a_k^{ij} H(\mathbf{r}'_k), \quad (8)$$

being N the total number of pixels. The same discretization of Eq. 3 can be obtained for P positions of the transducer and for I instants, in a way that a system of linear equations can be formulated, which is expressed in a matrix form as

$$\mathbf{p} = \mathbf{A}\mathbf{H}. \quad (9)$$

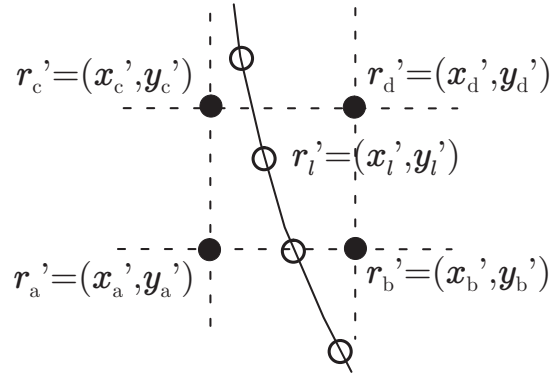


Figure 2. Bilinear interpolation of the optical absorbed energy at \mathbf{r}'_i as a function of the four neighbouring pixels of the ROI.

Eq. 9 corresponds to the forward model, in which the theoretical pressure for a set of detector positions and instants \mathbf{p} is calculated as a function of the absorbed energy in the pixel positions \mathbf{H} . The optoacoustic reconstruction is performed by minimizing the mean square difference between the theoretical pressure \mathbf{p} and the measured pressure \mathbf{p}_m , i.e.,

$$\mathbf{H}_{\text{sol}} = \underset{\mathbf{H}}{\text{argmin}} \|\mathbf{p}_m - \mathbf{A}\mathbf{H}\|^2. \quad (10)$$

The solution of Eq. 10 is calculated by means of the LSQR algorithm, in which the sparsity of the model matrix is exploited to make a fast reconstruction.

3. CORRECTION FOR ACOUSTIC ATTENUATION IN THE OPTOACOUSTIC SIGNALS

In a uniform attenuating medium, each frequency component of the pressure field $\tilde{p}(\mathbf{r}, \omega)$ satisfies the wave equation in the frequency domain (Helmholtz equation), i.e.,

$$\nabla^2 \tilde{p}(\mathbf{r}, \omega) + \hat{k}^2 \tilde{p}(\mathbf{r}, \omega) = S(\mathbf{r}, \omega), \quad (11)$$

where $S(\mathbf{r}, \omega)$ represents the acoustic sources and \hat{k} is the complex wavenumber defined as

$$\hat{k} = \frac{\omega}{c(\omega)} - j\alpha(\omega), \quad (12)$$

where $c(\omega)$ is the phase velocity and $\alpha(\omega)$ the attenuation coefficient. It has been established empirically that the attenuation coefficient in a wide variety of lossy media satisfies a power law dependence on frequency of the form

$$\alpha(\omega) = \alpha_{0\omega} |\omega|^n = \alpha_{0f} |f|^n, \quad (13)$$

being n a real positive constant and $\alpha_{0\omega}$ or α_{0f} the attenuation constant. For many biological tissues, $n \approx 1$ for the frequency range of ultrasonic imaging, and the average attenuation coefficient is $\alpha_{0f} \approx 0.5 \text{ dB MHz}^{-1} \text{ cm}^{-1}$. In such case, the dependence of the phase velocity on frequency is determined by the Kramers-Kronig relationships in order to guarantee causality. Thereby, the dispersion of the waves is given as a function of the phase velocity $c(\omega_0)$ at a reference angular frequency ω_0 as²⁰

$$\frac{1}{c(\omega)} = \frac{1}{c(\omega_0)} - \frac{2}{\pi} \alpha_{0\omega} \ln \left| \frac{\omega}{\omega_0} \right|. \quad (14)$$

The solution of Eq. 11 for a point source located at the origin, i.e. $S(\mathbf{r}, \omega) = \delta(\mathbf{r})$ in a 3D domain is given by

$$\tilde{p}(\mathbf{r}, \omega) = \frac{-1}{4\pi|\mathbf{r}|} \exp\left(-j\frac{\omega}{c(\omega_0)}|\mathbf{r}|\right) \exp[j\gamma(\omega)|\mathbf{r}|] = \tilde{p}_0(\mathbf{r}, \omega) \exp[j\gamma(\omega)|\mathbf{r}|], \quad (15)$$

where $\tilde{p}_0(\mathbf{r}, \omega)$ is the equivalent solution for a non-attenuating medium and $\gamma(\omega)$ is given by

$$\gamma(\omega) = \omega \left[\frac{1}{c(\omega_0)} - \frac{1}{c(\omega)} \right] - j\alpha(\omega). \quad (16)$$

The parameter $\gamma(\omega)$ has two components, $-j\alpha(\omega)$ corresponds to the correction of the reduction of amplitude of the Fourier spectrum components of the signal, whereas $\omega[1/c(\omega_0) - 1/c(\omega)]$ represents the correction of the effects of the dispersion associated with attenuation, which causes a change in the phase of the Fourier spectrum. In Ref. 18, we show that in practical situations no significant improvement is achieved if the phase is corrected, so that $\gamma(\omega)$ can be taken as

$$\gamma(\omega) \approx -j\alpha(\omega). \quad (17)$$

Then, the correction of the attenuation effects in an optoacoustic signal is done by correcting each frequency component with Eqs. 15 and 17, so that the equivalent signal for a non-attenuating medium is obtained, and then the reconstruction can be made with standard algorithms derived for ideal acoustic media.

4. EXPERIMENT

In the experiment we tested the correction of the signals originated at a phantom with embedded microparticles collected with and without an attenuating sample in the setup. The tomographic reconstruction yielded with the model-based scheme described in section 2 with the signals corrected for attenuation effects is then compared to the equivalent tomographic reconstruction yielded with the signals collected without the attenuating sample.

4.1 Experimental setup

The experimental setup consisted of an optical parametric oscillator (OPO)-based laser (MOPO series, Spectra Physics), pumped by a nanosecond pulsed Nd:YAG laser (Lab-190-30, Spectra-Physics) with 15 Hz pulse repetition, which is used as the illuminating source at a wavelength of 605 nm. The output laser beam was shaped in order to achieve ring-type uniform illumination conditions on the surface of the phantom. A cylindrically-focused ultrasonic immersion PZT transducer (model V382, Panametrics-NDT, Waltam, MA) with a center frequency of 7.5 MHz and a focal length of 25.4 mm was used to collect the time-resolved signals, which are then band-pass filtered with cut-off frequencies of 0.25 and 15 MHz. The sample is rotated with a high speed rotation stage (Thorlabs PRM1/M-Z7) with angular steps of 2° along a whole circumference, so that 180 tomographic projections are acquired. More details on the experimental setup can be found in Ref. 21.

The imaging phantom consisted of a 3 mm cylinder of pure agar solution (1.3% agar powder by weight). Polyethylene microparticles with an approximately diameter of 50 μm were inserted in the imaged slice of the phantom as optical absorbers.

A pork fat sample with a thickness of 7 mm was used as attenuating material. The signals were collected in two possible scenarios, namely with and without the attenuating sample in between the phantom and the transducer.

4.2 Experimental results

The optoacoustic signals collected with no acoustic attenuation are displayed in the first column of Fig. 3. The equivalent signals acquired by placing the attenuating sample in the setup are shown in the second column of Fig. 3. The reduction of amplitude and the broadening can be perceived by comparing the signals. The third column of Fig. 3 displays the signals collected with acoustic attenuation after being corrected with Eqs. 15 and 17. A low pass filter with a cutoff frequency of 9.5 MHz is applied in the Fourier spectra of the signals after correction in order to avoid the amplification of the high frequency noise.¹⁸ In fact, whereas the signals are

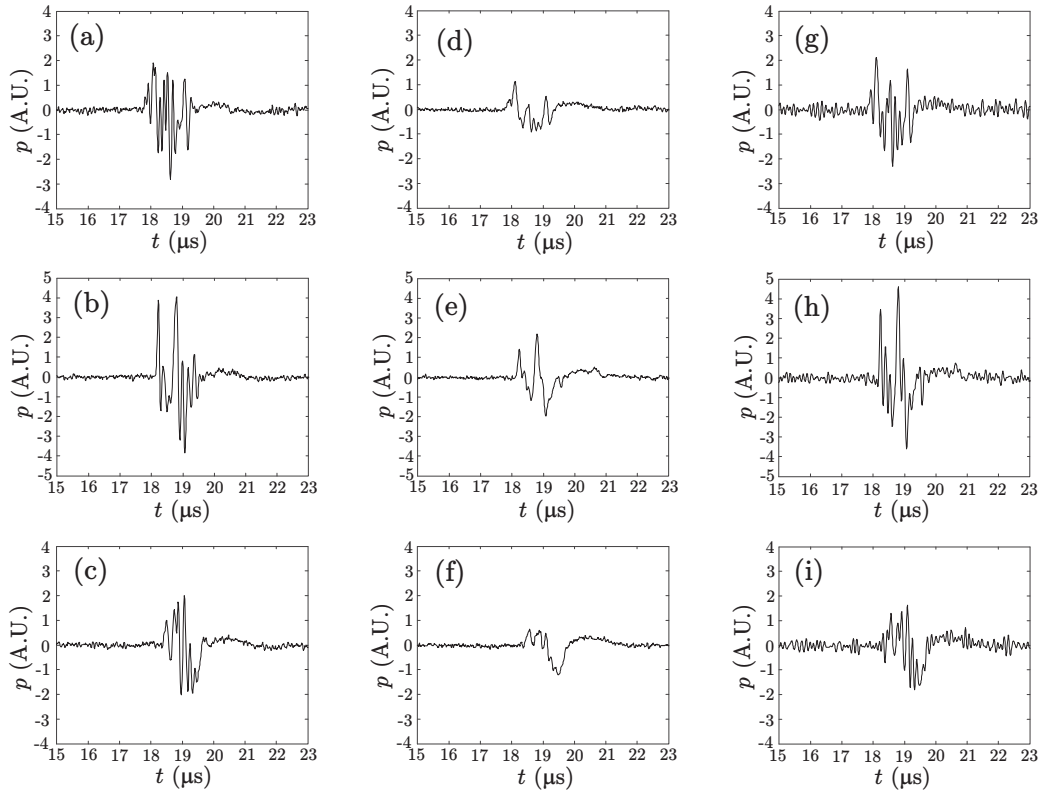


Figure 3. Optoacoustic signals corresponding to the imaging phantom acquired without acoustic attenuation (a-c) and by placing an attenuating sample in the setup (d-f) respectively. The respective signals corrected for the effects of acoustic attenuation are displayed in (g-i). The angular positions of the transducer are 28° , 58° and 106° for the first, second and third rows respectively.

improved in terms of correction of the reduction of amplitude and broadening, the corrected signals are noisier than the original ones. This is due to the amplification of the noise at relatively high frequencies. On the other hand, if a low pass filter with a lower cutoff frequency is used, the frequency spectra of the corrected signals are narrower and so the correction of amplitude and width of the signals is worse. Then, the cutoff frequency of the low pass filter must be selected according to the trade-off between performance of the correction and minimization of the noise.

Fig. 4 shows the tomographic reconstructions rendered by the model-based inversion algorithm for the three possible signals described above. The reduction of amplitude and broadening of the signals relate, respectively, to quantification inaccuracies and to loss of resolution in the reconstructed images. Both effects are clear by comparing the tomographic reconstruction obtained with the signals acquired with no attenuation (Fig. 4a) with the tomographic reconstruction obtained with the signals acquired with the attenuating sample in the setup (Fig. 4b). Specifically, Fig. 5 shows the profiles A and B indicated in Fig. 4a, where the reduction of amplitude and loss of resolution of the reconstructed optical absorbed energy are clearly perceived. Fig. 4c corresponds to the tomographic reconstruction obtained with the signals corrected for the effects of acoustic attenuation. In the corresponding profiles one can see that the reduction of amplitude and loss of resolution are partially corrected. However, the attenuation correction leads to the amplification of the background noise, specifically corresponding to relatively high spatial frequencies (Fig. 4c). Thus, the low pass filter applied to the signals after correction establishes the trade-off between the correction of quantification inaccuracies and resolution and the presence of background noise in the images.

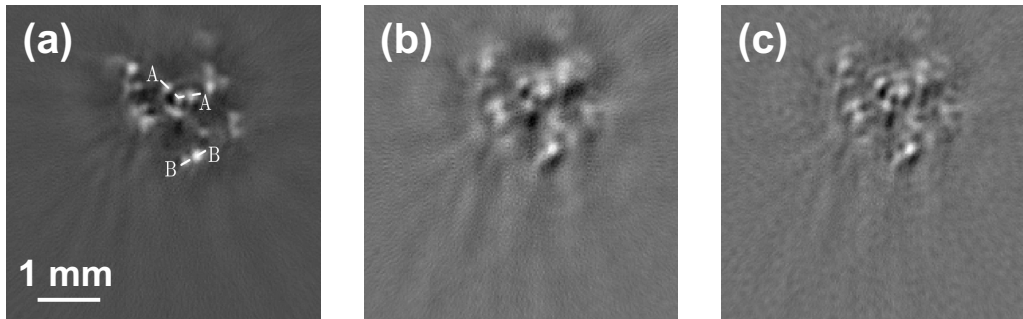


Figure 4. Tomographic reconstructions obtained with the model-based inversion algorithm by taking the signals acquired without acoustic attenuation (a) and the signals collected by placing an attenuating sample in the setup (b) respectively. The tomographic reconstruction obtained with the signals corrected for the effects of acoustic attenuation is shown in (c).

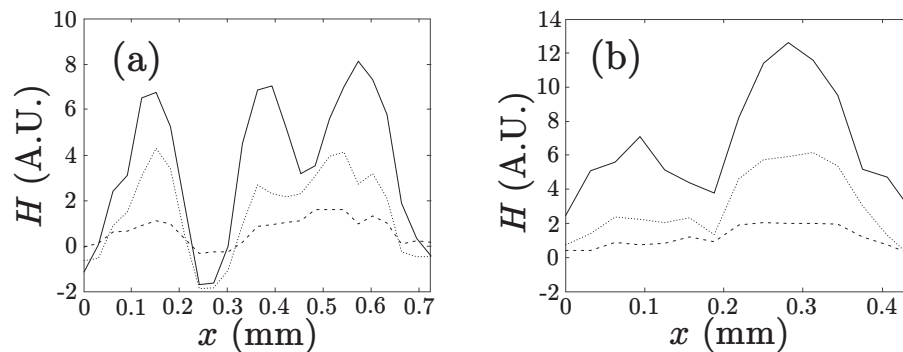


Figure 5. Profiles A (a) and B (b) of Fig. 4. The continuous, dashed and dotted lines correspond, respectively, to Figs. 4a, 4b and 4c.

5. CONCLUSIONS

In this work we have compared the optoacoustic tomographic reconstructions yielded with a model-based inversion algorithm in three possible scenarios, namely by considering the signals acquired with no acoustic attenuation, by considering the signals acquired with acoustic attenuation and by considering the signals corrected for the acoustic attenuation effects. The model-based scheme for making the reconstruction and the procedure to correct for acoustic attenuation effects were reviewed. Then, the correction for acoustic attenuation effects in the tomographic reconstructions was tested by imaging an agar phantom with embedded microparticles by placing an attenuation sample in between such phantom and the ultrasonic transducer. The results show that the quantification inaccuracies and the loss of resolution of the images can be partially corrected at the expense of introducing some noise due to the amplification of the high frequency components of the noise in the signals.

ACKNOWLEDGMENTS

D.R. acknowledges support from the German Research Foundation (DFG) Research Grant (RA 1848/1) and the European Research Council (ERC) Starting Grant. V.N. acknowledges support from the ERC Advanced Investigator Award and the German Ministry of Education (BMBF) Innovation in Medicine Award.

REFERENCES

- [1] Wang, X., Pang, Y., Ku, G., Xie, X., Stoica, G., and Wang, L. V., "Noninvasive laser-induced photoacoustic tomography for structural and functional *in vivo* imaging of the brain," *Nature Biotechnology* **21**(7), 803–806 (2003).
- [2] Razansky, D., Distel, M., Vinegoni, C., Ma, R., Perrimon, N., Köster, R. W., and Ntziachristos, V., "Multispectral opto-acoustic tomography of deep-seated fluorescent proteins *in vivo*," *Nature Photonics* **3**(7), 412–417 (2009).

- [3] Ntziachristos, V. and Razansky, D., “Molecular imaging by means of multispectral optoacoustic tomography (MSOT),” *Chemical Reviews* **110**(5), 2783–2794 (2010).
- [4] Wang, L. V., ed., [*Photoacoustic Imaging and Spectroscopy*], CRC Press, Boca Raton (USA) (2009).
- [5] Kruger, R. A., Liu, P., Fang, Y., and Appledorn, C. R., “Photoacoustic ultrasound PAUS - reconstruction tomography,” *Medical Physics* **22**(10), 1605–1609 (1995).
- [6] Köstli, K. P., Frenz, M., Bebie, H., and Weber, H. P., “Temporal backward projection of optoacoustic pressure transients using fourier transform methods,” *Physics in Medicine and Biology* **46**(7), 1863–1872 (2001).
- [7] Norton, S. J. and Vo-Dinh, T., “Optoacoustic diffraction tomography: analysis of algorithms,” *Journal of the Optical Society of America A* **20**(10), 1859–1866 (2003).
- [8] Rosenthal, A., Razansky, D., and Ntziachristos, V., “Fast semi-analytical model-based acoustic inversion for quantitative optoacoustic tomography,” *IEEE Transactions on Medical Imaging* **29**(6), 1275–1285 (2010).
- [9] Xu, Y. and Wang, L. V., “Effects of acoustic heterogeneity in breast thermoacoustic tomography,” *IEEE Transactions on Ultrasonics, Ferroelectrics and Frequency Control* **50**(9), 1134–1146 (2003).
- [10] Deán-Ben, X. L., Ma, R., Razansky, D., and Ntziachristos, V., “Statistical approach for optoacoustic image reconstruction in the presence of strong acoustic heterogeneities,” *IEEE Transactions on Medical Imaging* **30**(2), 401–408 (2011).
- [11] Jin, X. and Wang, L. V., “Thermoacoustic tomography with correction for acoustic speed variations,” *Physics in Medicine and Biology* **51**(24), 6437–6448 (2006).
- [12] Jiang, H., Yuan, Z., and Gu, X., “Spatially varying optical and acoustic property reconstruction using finite-element-based photoacoustic tomography,” *Journal of the Optical Society of America A* **23**(4), 878–888 (2006).
- [13] Deán-Ben, X. L., Ntziachristos, V., and Razansky, D., “Statistical optoacoustic image reconstruction using a-priori knowledge on the location of acoustic distortions,” *Applied Physics Letters* (2011). DOI:10.1063/1.3564905.
- [14] Szabo, T. L., [*Diagnostic Ultrasound Imaging: Inside Out*], Elsevier Academic Press, San Diego (USA) (2004).
- [15] Nussenzveig, H. M., [*Causality and Dispersion Relations*], Academic Press, New York (USA) (1972).
- [16] Patch, S. K. and Greenleaf, A., “Ultrasound attenuation and thermo/photo/opto-acoustic tomography - theoretical foundation,” *Proceedings of SPIE* **6437**, 643726 (2007).
- [17] Treeby, B. E. and Cox, B. T., “Fast, tissue-realistic models of photoacoustic wave propagation for homogeneous attenuating media,” *Proceedings of SPIE* **7177**, 717716 (2009).
- [18] Deán-Ben, X. L., Razansky, D., and Ntziachristos, V., “Effects of acoustic attenuation in optoacoustic signals,” (Under review).
- [19] Gusev, V. E. and Karabutov, A. A., [*Laser Optoacoustics*], American Institute of Physics, New York (USA) (1993).
- [20] Sushilov, N. V. and Cobbold, R. S. C., “Frequency-domain wave equation and its time-domain solutions in attenuating media,” *Journal of the Acoustical Society of America* **115**(4), 1431–1436 (2004).
- [21] Ma, R., Taruttis, A., Ntziachristos, V., and Razansky, D., “Multispectral optoacoustic tomography (MSOT) scanner for whole-body small animal imaging,” *Optics Express* **17**(24), 21414–21426 (2009).